

# Dispersive analysis of neutral meson mixing

Hsiang-nan Li

*Institute of Physics, Academia Sinica, Taipei, Taiwan 115, Republic of China*

(Dated: March 9, 2023)

We analyze the neutral meson mixing by directly solving the dispersion relation obeyed by the mass and width differences of the two meson mass eigenstates. We solve for the parameters  $x$  and  $y$ , proportional to the mass and width differences in the charm mixing, respectively, taking the box-diagram contributions to  $x(s)$  and  $y(s)$  at large mass squared  $s$  of a fictitious  $D$  meson as inputs. The SU(3) symmetry breaking is introduced through physical thresholds of different  $D$  meson decay channels for  $y(s)$ . These threshold-dependent effects, acting like nonperturbative power corrections in QCD sum rules, stabilize the solutions of  $y(s = m_D^2)$  with the  $D$  meson mass  $m_D$ . We then calculate  $x(s)$  through the dispersive integration of  $y(s)$ , and show that our predictions  $x(m_D^2) \approx 0.21\%$  and  $y(m_D^2) \approx 0.52\%$  are close to the data in both  $CP$ -conserving and  $CP$ -violating cases. It is observed that the channel containing di-kaon states provides the major source of SU(3) breaking, which enhances  $x(m_D^2)$  and  $y(m_D^2)$  by four orders of magnitude relative to the perturbative results. We also predict the coefficient ratio  $q/p$  involved in the charm mixing with  $|q/p|-1 \approx 2 \times 10^{-4}$  and  $Arg(q/p) \approx 6 \times 10^{-3}$  degrees, which can be scrutinized by precise future measurements. The formalism is extended to studies of the  $B_{s(d)}$  meson mixing and the kaon mixing, and the small deviations of the obtained width differences from the perturbative inputs explain why the above mixing can be understood via short-distance dynamics. We claim that the puzzling charm mixing is attributed to the strong Glashow-Iliopoulos-Maiani suppression on perturbative contributions, instead of to breakdown of the quark-hadron duality, which occurs only at 15% level.

## I. INTRODUCTION

It has been a long-standing challenge to understand the observed large  $D$  meson mixing, which is manifested by the parameters  $x$  and  $y$  of order of  $10^{-3}$  [1]. The former (latter) is defined in terms of the mass (width) difference between the two neutral  $D$  meson mass eigenstates. The inclusive analyses based on the heavy quark effective field theory [2, 3] led to tiny  $x$  and  $y$  due to the strong Glashow-Iliopoulos-Maiani (GIM) suppression [4]. The inclusion of next-to-leading-order QCD corrections yielded  $x \sim y \simeq 6 \times 10^{-7}$  [5], which fall short of the experimental data by four orders of magnitude. It was speculated [6–8] that contributions from higher dimensional operators might circumvent the GIM suppression, and enhance  $x$  and  $y$  significantly. This speculation, requiring information on numerous nonperturbative matrix elements, has not been verified quantitatively. On the other hand, the exclusive analyses, where the mixing parameter  $y$  is extracted from data of hadronic  $D$  meson decays [7, 9–18], accounted for a half value of  $y$  roughly by summing up the contributions from two-body modes [16, 18]. However, it is difficult to estimate the effects from other multi-body decays and to explain  $x$  and  $y$  simultaneously in this data-driven approach. For recent reviews on the charm mixing and related subjects, refer to [19, 20].

The above challenge has motivated our proposal to study the  $D$  meson mixing as an inverse problem, i.e., to solve the dispersion relation obeyed by  $x(s)$  and  $y(s)$  for a fictitious  $D$  meson with an arbitrary mass squared  $s$  [21]. The function  $y(s)$  was separated into a high-mass piece and a low-mass piece, with the former and  $x(s)$  at large  $s$  being input from reliable perturbative computations of the box diagrams [22–24]. The latter, treated as an unknown, was derived from the integral equation constructed from the dispersion relation. The unknown piece of  $y(s)$  was parametrized, and the involved parameters were fixed by the best fit of its dispersive integral to the perturbative input. It turned out that many solutions of  $y(s)$ , corresponding to minima of the fit, were allowed as a consequence of the ill posed nature of an inverse problem, and those matching the data were selected. Strictly speaking, the large  $x$  and  $y$  obtained in [21] are not an unambiguous prediction. The point is instead to demonstrate the existence of the nontrivial correlated solutions for  $x$  and  $y$ , which, with magnitudes being much greater than from the box diagrams [25], accommodate the large  $D$  meson mixing. Nevertheless, the attempt in [21] based only on the analyticity of physical observables is novel, and has been extended to the constraint on the hadronic vacuum polarization contribution to the muon anomalous magnetic moment [26] and to the reformulation of QCD sum rules for determining properties of the series of  $\rho$  resonances [27], glueball masses [28] and the pion light-cone distribution amplitude [29].

We will improve our previous work on the charm mixing [21] by solving the dispersion relation directly, which sets a stringent connection between the mixing parameters  $x(s)$  and  $y(s)$ , without relying on a discretionary parametrization. The advantage of the inverse matrix method developed in [28] is that a unique and stable solution can be attained before an ill posed nature appears. The inputs  $x(s)$  and  $y(s)$  at large  $s$  come from the perturbative contributions, which have been known to explain the observed  $B_{(s)}$  meson mixing satisfactorily [30–35]. It has been noticed that the  $D$  meson mixing, strongly suppressed by the GIM mechanism, is sensitive to nonperturbative SU(3) symmetry breaking

effects [36] characterized by the strange and down quark mass difference, and to Cabibbo-Kobayashi-Maskawa (CKM)-suppressed diagrams with bottom quarks in the loop. In our formalism the SU(3) breaking is introduced through physical thresholds for  $y(s)$ , which depend on final states of  $D$  meson decays, such as  $4m_K^2$  for the channel involving two strange quarks,  $m_K$  being the kaon mass. It will be illustrated that these threshold-dependent pieces play a role of nonperturbative condensate, i.e., power corrections in QCD sum rules [37], which stabilize the solutions of  $y(s = m_D^2)$  solved from the above inverse problem,  $m_D$  being the  $D$  meson mass. The function  $x(s)$  is then derived via the dispersive integration of the obtained  $y(s)$  straightforwardly. We find that the results of  $x(m_D^2)$  and  $y(m_D^2)$  are consistent with the data in the  $CP$ -conserving case, as reasonable values for the bag parameter and the mass ratio  $m_D/m_c$  associated with the  $(S - P)(S - P)$  effective  $\Delta C = 2$  operator are considered, where  $m_c$  is the charm quark mass, and  $S$  ( $P$ ) denotes the scalar (pseudoscalar) current.

It will be shown that the solution of  $y(s)$  from the dispersion relation does not deviate from the corresponding input much for each  $D$  meson decay channel actually. In other words, the quark-hadron duality assumed in the inclusive calculations is not broken severely for individual channel. The contributions from the channel containing two down quarks and the channel containing one down quark and one strange quark remain similar, and cancel approximately. The channel with two strange quarks, i.e., di-kaon states, provides the major source of the SU(3) breaking, which enhances the net contribution to  $y(m_D^2)$  from all channels by four orders of magnitude relative to the perturbative one. Our observation supports the postulation [35] that a modest duality violation of about 20% accounts for the huge distinction between the data and the predictions for the charm mixing in the inclusive analyses. Once the solutions of  $x(s)$  and  $y(s)$  for each channel are available, it is straightforward to investigate  $CP$  violation in the mixing by considering the imaginary parts of the CKM matrix elements. It will be seen that the resultant  $x(m_D^2)$  and  $y(m_D^2)$  are close to the data in the  $CP$ -violating case, after the reasonable matrix element of the  $(S - P)(S - P)$  operator is taken into account. At the same time, we predict the ratio  $q/p$ , where  $p$  and  $q$  are the coefficients relating the  $D$  meson mass eigenstates to the flavor eigenstates through a linear combination. The prediction can be confronted by precise future measurements, and employed to constrain new physics models.

We then extend the formalism to studies of the  $B_{s(d)}$  meson mixing and the kaon mixing. As mentioned before, the former can be well described in heavy quark expansion [30–33]. The latter has been also explored intensively in perturbation theory based on the effective Hamiltonian, and the relevant data have been understood to some extent [38–40]. For example, it was demonstrated [40] that short-distance contributions amount up to 89% of the measured mass difference for the kaon mixing. Hence, we do not aim at precise evaluations for the above neutral meson mixing, but at a general picture on the mixing mechanism, and argue that they can be addressed in our framework consistently and systematically. As expected, the solution of the width difference is roughly equal to the corresponding input for each involved decay channel, similar to what is found in the  $D$  meson case. The major variation originates from the CKM matrix elements and the phase space allowed for decay channels. It is obvious that the GIM suppression is less effective in the  $B_{s(d)}$  meson mixing with the different CKM factors for the up and charm quark channels. The GIM suppression is absent in the kaon mixing, because only the up quark channel survives the phase space constraint. We thus claim that the puzzling  $D$  meson mixing, in contrast to the others, is attributed to the strong GIM suppression on the perturbative contributions in the inclusive analyses, instead of to breakdown of the quark-hadron duality.

The rest of the paper is organized as follows. In Sec. II we start with the dispersion relation between the mixing parameters  $x(s)$  and  $y(s)$  for a fictitious  $D$  meson, and establish the integral equation for the unknown function  $y(s)$  that incorporates appropriate boundary conditions at physical thresholds of involved decay channels. The SU(3) symmetry breaking effects which mimic nonperturbative power corrections in QCD sum rules are identified. The inverse matrix method to solve the integral equation is also elaborated on. The equation is solved in Sec. III with the perturbative inputs from the box diagrams responsible for the charm mixing. The solution for  $y(s)$  is determined, via whose dispersive integration the unknown function  $x(s)$  is derived. The stability and reliability of the obtained  $x(m_D^2)$  and  $y(m_D^2)$  are justified. Our predictions for the relevant observables in both the  $CP$ -conserving and  $CP$ -violating cases are presented. We repeat the above procedures to the  $B_{s(d)}$  meson mixing and the kaon mixing, and highlight the uniqueness of the  $D$  meson mixing in Sec. IV. Section V contains the conclusion and outlook.

## II. FORMALISM

The dispersive piece  $M_{12}(s)$  and the absorptive piece  $\Gamma_{12}(s)$  of the analytical transition matrix elements, which govern the time evolution of a fictitious  $D$  meson of invariant mass squared  $s$ , satisfy the dispersion relation [15]

$$M_{12}(s) = \frac{1}{2\pi} \int_{4m_\pi^2}^{\infty} ds' \frac{\Gamma_{12}(s')}{s - s'}, \quad (1)$$

where the application of the principal-value prescription to the right-hand side is implicit, and  $4m_\pi^2$  with the pion mass  $m_\pi$  is the threshold for hadronic  $D$  meson decays. The mass eigenstates  $|D_{1,2}\rangle = p|D^0\rangle \pm q|\bar{D}^0\rangle$  are written as

the linear combinations of the flavor eigenstates  $D^0$  and  $\bar{D}^0$  with the coefficient ratio

$$\frac{q}{p} = \sqrt{\frac{2M_{12}^* - i\Gamma_{12}^*}{2M_{12} - i\Gamma_{12}}}. \quad (2)$$

We adopt the phase convention  $CP|D^0\rangle = -|\bar{D}^0\rangle$  for the  $CP$  transformation. The mass and width differences of the  $D_{1,2}$  mesons define the mixing parameters [41]

$$x \equiv \frac{m_2 - m_1}{\Gamma} = \frac{1}{\Gamma} \text{Re} \left[ \frac{q}{p} (2M_{12} - i\Gamma_{12}) \right], \quad y \equiv \frac{\Gamma_2 - \Gamma_1}{2\Gamma} = -\frac{1}{\Gamma} \text{Im} \left[ \frac{q}{p} (2M_{12} - i\Gamma_{12}) \right], \quad (3)$$

with the total decay width  $\Gamma$ , which reduce to

$$x = \frac{2M_{12}}{\Gamma}, \quad y = \frac{\Gamma_{12}}{\Gamma}, \quad (4)$$

in the  $CP$ -conserving case. The masses of the other quarks maintain their physical values, so the fictitious  $D$  meson decays into the allowed final states, as its mass crosses each threshold.

We decompose the absorptive piece into

$$\Gamma_{12}(s) = \sum_{i,j} \lambda_i \lambda_j \Gamma_{ij}(s), \quad (5)$$

with the internal quarks  $i, j = d, s, b$ , and  $\lambda_k \equiv V_{ck} V_{uk}^*$ ,  $k = d, s, b$ , being the products of the CKM matrix elements. The component  $\Gamma_{ij}(s)$ , calculable perturbatively at large  $s$ , approaches the box-diagram contribution

$$\Gamma_{ij}^{\text{box}}(s) = \frac{G_F^2 f_D^2 m_W^3 B_D}{12\pi^2} A_{ij}^{\text{box}}(s), \quad (6)$$

where  $G_F$  is the Fermi constant,  $f_D$  is the  $D$  meson decay constant,  $m_W$  is the  $W$  boson mass and  $B_D$  is the bag parameter. The perturbative function  $A_{ij}^{\text{box}}$  combines the results from the  $(V - A)(V - A)$  and  $(S - P)(S - P)$  operators in the effective weak Hamiltonian [23],

$$A_{ij}^{\text{box}}(s) = \frac{\pi}{2x_D^{3/2}} \frac{\sqrt{x_D^2 - 2x_D(x_i + x_j) + (x_i - x_j)^2}}{(1 - x_i)(1 - x_j)} \times \left\{ \left( 1 + \frac{x_i x_j}{4} \right) [3x_D^2 - x_D(x_i + x_j) - 2(x_i - x_j)^2] + 2x_D(x_i + x_j)(x_i + x_j - x_D) \right\}, \quad (7)$$

which is symmetric under the exchange of the subscripts  $i$  and  $j$ , i.e.,  $A_{ij}^{\text{box}}(s) = A_{ji}^{\text{box}}(s)$ . We have flipped the sign of the formula in [23] to match the convention in Eq. (3). In the above expression the variables are defined as  $x_i = m_i^2/m_W^2$ ,  $m_i$  being the mass of the quark  $i$ , and  $x_D = s/m_W^2$ . Note that  $A_{ij}^{\text{box}}$  contribute up to  $A_{dd}^{\text{box}}$  ( $A_{ds}^{\text{box}}$ ,  $A_{ss}^{\text{box}}$ ,  $A_{db}^{\text{box}}$ ,  $A_{sb}^{\text{box}}$ ,  $A_{bb}^{\text{box}}$ ) allowed in the range  $s < (m_d + m_s)^2$  [ $(m_d + m_s)^2 \leq s < 4m_s^2$ ,  $4m_s^2 \leq s < (m_d + m_b)^2$ ,  $(m_d + m_b)^2 \leq s < (m_s + m_b)^2$ ,  $(m_s + m_b)^2 \leq s < 4m_b^2$ ,  $4m_b^2 \leq s$ ].

Similarly, we decompose the dispersive piece into  $M_{12}(s) = \sum_{i,j} \lambda_i \lambda_j M_{ij}(s)$ . In principle, the dispersion relation, as a result of QCD dynamics which has nothing to do with the CKM factors, holds for each pair of the components  $M_{ij}(s)$  and  $\Gamma_{ij}(s)$ . This fact has been noticed in [21], but was not implemented in the preliminary attempt there. Though  $\Gamma_{12}(s)$  decreases fast enough at large  $s$  [21], so that the dispersive integral on the right hand side of Eq. (1) converges, each component  $\Gamma_{ij}(s)$  grows like  $s^{3/2}$  as indicated in Eq. (7). These divergent behaviors cancel in the sum in Eq. (5), when the unitarity of the CKM factors is imposed. We thus reformulate the dispersion relation, starting with the contour integral for the analytical function  $\Pi_{ij}(s) = M_{ij}(s) - i\Gamma_{ij}(s)/2$ ,

$$\frac{1}{2\pi i} \oint ds' \frac{\Pi_{ij}(s')}{s - s'} = 0. \quad (8)$$

The contour in Eq. (8) consists of two pieces of horizontal lines above and below the branch cut along the positive real axis on the complex  $s'$  plane, a circle of small radius  $r$  around the pole  $s' = s$  located on the positive real axis, and a circle  $C_R$  of large radius  $R$  as depicted in Fig. 1. The integral vanishes, since there is no pole in the contour, which encloses only unphysical regions. The contribution along the small clockwise circle yields  $M_{ij}$ , and that from the two pieces of horizontal lines leads to the dispersive integral of  $\Gamma_{ij}$ . Equation (8) then gives

$$M_{ij}(s) = \frac{1}{2\pi} \int_{m_{IJ}}^R ds' \frac{\Gamma_{ij}(s')}{s - s'} + \frac{1}{2\pi i} \int_{C_R} ds' \frac{\Pi_{ij}^{\text{box}}(s')}{s - s'}, \quad (9)$$

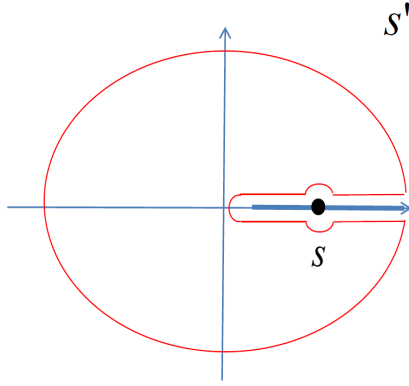


FIG. 1: Contour considered in Eq. (8), where the thick line represents the branch cut.

where  $m_{IJ}$  represents the threshold mass squared of the hadronic states contributing to  $\Gamma_{ij}$ , such as  $m_{\pi\pi} = 4m_\pi^2$ ,  $m_{\pi K} = (m_\pi + m_K)^2$ ,  $m_{KK} = 4m_K^2$ ,  $m_{\pi B} = (m_\pi + m_B)^2$ , ... with the  $B$  meson mass  $m_B$ . The unknown function  $\Gamma_{ij}(s)$ , containing nonperturbative dynamics from the low  $s$  region, will be solved from the dispersion relation. The integrand  $\Pi_{ij}$ , taking values along the large clockwise circle  $C_R$ , can be safely replaced by the perturbative expression  $\Pi_{ij}^{\text{box}}$  from the box-diagram computation.

The dispersive piece  $M_{ij}^{\text{box}}(s)$  and the absorptive piece  $\Gamma_{ij}^{\text{box}}(s)$  associated with the box diagrams respect the dispersion relation apparently,

$$M_{ij}^{\text{box}}(s) = \frac{1}{2\pi} \int_{m_{ij}}^R ds' \frac{\Gamma_{ij}^{\text{box}}(s')}{s-s'} + \frac{1}{2\pi i} \int_{C_R} ds' \frac{\Pi_{ij}^{\text{box}}(s')}{s-s'}, \quad (10)$$

where  $m_{ij}$  is the threshold mass squared of the quark states contributing to  $\Gamma_{ij}^{\text{box}}$ , such as  $m_{dd} = 4m_d^2$ ,  $m_{ds} = (m_d + m_s)^2$ ,  $m_{ss} = 4m_s^2$ ,  $m_{db} = (m_d + m_b)^2$ , .... Because a heavy neutral meson mixing can be well described by perturbative contributions, we approximate  $M_{ij}(s)$  by  $M_{ij}^{\text{box}}(s)$ , i.e., equate Eqs.(9) and (10) at large enough  $s$ , arriving at

$$\int_{m_{IJ}}^R ds' \frac{\Gamma_{ij}(s')}{s-s'} = \int_{m_{ij}}^R ds' \frac{\Gamma_{ij}^{\text{box}}(s')}{s-s'}, \quad (11)$$

where the box-diagram contributions from the large circle  $C_R$  on the two sides have canceled.

It has been emphasized [28] that the boundary condition of an unknown function is crucial for the determination of its solutions from a dispersion relation. As  $s$  is near a threshold, the fictitious  $D$  meson decay is dominated by a single mode  $D \rightarrow PP$ , with  $P$  representing a light pseudoscalar meson of mass  $m_P$ . For instance, the components  $\Gamma_{dd}$ ,  $\Gamma_{ds}$ , and  $\Gamma_{ss}$  are dominated by  $D \rightarrow \pi\pi$ ,  $\pi K$ , and  $KK$ , respectively, when the fictitious  $D$  meson mass approaches the corresponding thresholds from above. The  $D \rightarrow PP$  decay width is proportional to  $p_c |\mathcal{M}|^2/s$ , with  $p_c$  being the center-of-mass momentum of the pseudoscalar meson, and the amplitude  $\mathcal{M} \propto s - m_P^2$  in the naive factorization assumption. It is then easy to acquire the power-law behaviors  $p_c \sim O(m_P)$ ,  $\mathcal{M} \sim O(m_P^2)$  and  $\Gamma_{ij} \sim O(m_P^3)$  around the threshold  $s \sim O(m_P^2)$ . The naive factorization assumption may not be reliable in the above low-mass regions, but it is interesting to note that the obtained observation is the same as deduced from the  $K \rightarrow \pi\pi$  amplitude in chiral perturbation theory [15]. Certainly, the above argument does not apply to the boundary conditions of the components  $\Gamma_{(d,s,b)b}$ , to which the states containing heavy  $B$  mesons contribute: the similar reasoning leads to  $\Gamma_{db} \sim \Gamma_{sb} \sim O(m_P)$  at  $s \sim (m_B + m_P)^2$ . Nevertheless, we will assume the same threshold behaviors for the derivations of  $\Gamma_{(d,s,b)b}$ , since their contributions to the  $D$  meson mixing are negligible owing to the strong suppression by the CKM factors as explicitly verified in the next section.

Following the procedure in [28], we introduce a subtracted unknown function  $\Delta\Gamma_{ij}$ , which is related to the original  $\Gamma_{ij}$  via

$$\Delta\Gamma_{ij}(s, \Lambda) = \Gamma_{ij}(s) - \Gamma_{ij}^{\text{box}}(s) \{1 - \exp[-(s - m_{IJ})^2/\Lambda^2]\}. \quad (12)$$

The scale  $\Lambda$  characterizes the order of  $s$ , at which  $\Gamma_{ij}(s)$  transits to the perturbative expression  $\Gamma_{ij}^{\text{box}}(s)$ . The subtraction term in Eq. (12) vanishes like  $(s - m_{IJ})^2 \sim O(m_{IJ}^2)$  near the threshold  $s \sim O(m_{IJ})$ , because  $\Gamma_{ij}^{\text{box}}(m_{IJ})$

with  $m_{IJ} > m_{ij}$  is finite as implied by Eq. (7). Namely,  $\Delta\Gamma_{ij}(s, \Lambda)$  exhibits the low-mass behavior the same as  $\Gamma_{ij}(s) \sim O(m_{IJ}^{3/2})$ . We have tested other choices of the subtraction function, like  $1 - \exp[-(s - m_{IJ})^3/\Lambda^3]$ , which diminishes more rapidly as  $s \rightarrow m_{IJ}$  and does not modify the low-mass behavior of  $\Gamma_{ij}(s)$  either, and made sure that our solutions for the mixing parameters alter by only few percent. The function  $1 - \exp[-(s - m_{IJ})^2/\Lambda^2]$  in Eq. (12) approaches unity, i.e.,  $\Delta\Gamma_{ij}(s, \Lambda)$  vanishes only at large  $s \gg \Lambda$ . In other words, the quark-hadron duality is not postulated at any finite  $s$  in our formalism.

The subtraction term in Eq. (12) can be regarded as an ultraviolet regulator for a dispersive integral mentioned in [42]. The dispersive integral, formulated with the subtracted unknown function, then converges, and Eq. (11) can be rewritten as

$$\int_{m_{IJ}}^{\infty} ds' \frac{\Delta\Gamma_{ij}(s', \Lambda)}{s - s'} = \int_{m_{IJ}}^{\infty} ds' \frac{\Gamma_{ij}^{\text{box}}(s') \exp[-(s' - m_{IJ})^2/\Lambda^2]}{s - s'} + \int_{m_{ij}}^{m_{IJ}} ds' \frac{\Gamma_{ij}^{\text{box}}(s')}{s - s'}, \quad (13)$$

where the upper bounds  $R$  have been pushed to infinity due to the finiteness of the integrals. Note that an emitted  $W$  boson can become real when  $s$  is large enough, and the expression of  $\Gamma_{ij}^{\text{box}}(s)$  should be modified. As observed in the next section, the scale  $\Lambda$  takes values of order of few  $\text{GeV}^2$ , so the concerned high-mass region, greatly suppressed by the exponential factor  $\exp[-(s' - m_{IJ})^2/\Lambda^2]$ , is not important. Strictly speaking, the decay constant  $f_D$  and the bag parameter  $B_D$  depend on the fictitious  $D$  meson mass. However, the decay constants of the physical pseudoscalar mesons do not vary much in the low  $s$  region, ranging from  $m_\pi^2 \approx 0.02 \text{ GeV}^2$  to  $m_{B_s}^2 \approx 29 \text{ GeV}^2$ , to which Eq. (13) is relevant. That is, the value of  $f_D$  does not matter to the explanation of the  $10^4$  enhancement factor. The bag parameters fluctuate only a bit in the range of  $s$  from  $m_K^2 \approx 0.25 \text{ GeV}^2$  to  $m_{B_s}^2 \approx 29 \text{ GeV}^2$  as shown in the lattice calculations [43–46]. Hence, it is numerically appropriate to treat both  $f_D$  and  $B_D$  as constants in the dominant  $s'$  region for Eq. (13).

We then remove the common constant prefactors on the two sides of Eq. (13), and replace  $\Delta\Gamma_{ij}(s, \Lambda)$  [ $\Gamma_{ij}^{\text{box}}(s)$ ] by the function  $\Delta A_{ij}(s, \Lambda)$  [ $A_{ij}^{\text{box}}(s)$ ] according to Eq. (6). Since  $\Delta A_{ij}(s, \Lambda)$  is a dimensionless quantity, it can be cast into the form  $\Delta A_{ij}(s/\Lambda)$ . Other ratios like  $s/m_{IJ}$  can be reexpressed as  $(s/\Lambda)(\Lambda/m_{IJ})$ , so  $s/\Lambda$  is the only variable of  $\Delta A_{ij}$ . Equation (13) becomes, under the substitution  $s' \rightarrow s' + m_{IJ}$  and the variable changes  $s - m_{IJ} = u\Lambda$ ,  $s' = v\Lambda$ ,  $m_{ij} = r_{ij}\Lambda$  and  $m_{IJ} = r_{IJ}\Lambda$ ,

$$\int_0^{\infty} dv \frac{\Delta A_{ij}(v)}{u - v} = \int_0^{\infty} dv \frac{A_{ij}^{\text{box}}(v\Lambda + m_{IJ})e^{-v^2}}{u - v} + \int_{r_{ij}-r_{IJ}}^0 dv \frac{A_{ij}^{\text{box}}(v\Lambda + m_{IJ})}{u - v}. \quad (14)$$

The lower bound of the second term on the right-hand side represents the sources of nonperturbative dynamics with  $m_{IJ} \neq m_{ij}$ , and of the SU(3) symmetry breaking with the dependence of  $m_{IJ}$  on the hadronic states labelled by  $IJ$ . The solutions for the mixing parameters, as physical observables, should be insensitive to the transition scale  $\Lambda$ , which is introduced through the ultraviolet regulation for the dispersive integrals. It will be elaborated that the second term on the right-hand side of Eq. (14) plays the role of nonperturbative condensate, i.e., power corrections in QCD sum rules, which stabilize the solutions with respect to the variation of  $\Lambda$ . When  $\Lambda$  increases, the magnitude of the first integral on the right-hand side grows, for  $A_{ij}^{\text{box}}$  behaves monotonically with  $s$ . On the contrary, the second integral picks up values of  $A_{ij}^{\text{box}}$  at lower  $s$  specified by the integration interval, where  $A_{ij}^{\text{box}}$  changes slowly. The shrinking of the integration interval with  $\Lambda$  yields stronger reduction, such that the magnitude of the second integral decreases. It is possible that the changes of the two terms compensate each other, and stable solutions may exist in a window of  $\Lambda$ , which are then identified as our results for the mixing parameters. The numerical analysis to be performed in the next section does reveal the stability of the solutions.

Viewing the boundary condition of  $\Delta A_{ij}(v) \sim v^{3/2}$  at  $v \rightarrow 0$ , we expand it in terms of the generalized Laguerre polynomials  $L_n^{(\alpha)}(v)$  for the parameter  $\alpha = 3/2$ ,

$$\Delta A_{ij}(v) = \sum_{n=1}^N a_n^{(ij)} v^\alpha e^{-v} L_{n-1}^{(\alpha)}(v), \quad (15)$$

up to degree  $N - 1$  with the unknown coefficients  $a_n^{(ij)}$ . The generalized Laguerre polynomials obey the orthogonality

$$\int_0^{\infty} v^\alpha e^{-v} L_m^{(\alpha)}(v) L_n^{(\alpha)}(v) dv = \frac{\Gamma(m + \alpha + 1)}{m!} \delta_{mn}. \quad (16)$$

The number of polynomials  $N$  should be as large as possible, such that Eq. (15) best describes the subtracted unknown function, but cannot be too large in order to avoid the appearance of an ill posed nature. Because  $\Delta A_{ij}(v)$  decreases

quickly enough with  $v$ , as designed in Eq. (12), the major contribution to its integral arises from a finite range of  $v$ . It is then justified to expand the integral on the left-hand side of Eq. (14) into a series in  $1/u$  up to the power  $N$  for a sufficiently large  $|u|$  by inserting

$$\frac{1}{u-v} = \sum_{m=1}^N \frac{v^{m-1}}{u^m}. \quad (17)$$

The right-hand side of Eq. (14) can be expanded into a power series in  $1/u$ : the exponential factor  $e^{-v^2}$  in the first integral diminishes the contribution from large  $v$ , and  $v$  is restricted in a finite interval in the second integral.

Substituting Eqs. (15) and (17) into Eq. (14), and equating the coefficients of  $1/u^m$  in the power series on the two sides of Eq. (14), we construct the matrix equation  $Ua^{(ij)} = b^{(ij)}$  with the matrix elements

$$U_{mn} = \int_0^\infty dv v^{m-1+\alpha} e^{-v} L_{n-1}^{(\alpha)}(v), \quad (18)$$

where  $m$  and  $n$  run from 1 to  $N$ . We have  $U_{mn} = 0$  actually for  $n > m$  with the orthogonality condition in Eq. (16). The vector

$$a^{(ij)} = (a_1^{(ij)}, a_2^{(ij)}, \dots, a_N^{(ij)}), \quad (19)$$

collects the unknowns. The power expansion on the right-hand side of Eq. (14) gives the coefficient  $b_m^{(ij)}$  of the term  $1/u^m$ , i.e., the  $m$ th element of the input vector  $b^{(ij)}$ ,

$$b_m^{(ij)} = \int_0^\infty dv v^{m-1} A_{ij}^{\text{box}}(v\Lambda + m_{IJ}) e^{-v^2} + \int_{r_{ij}-r_{IJ}}^0 dv v^{m-1} A_{ij}^{\text{box}}(v\Lambda + m_{IJ}). \quad (20)$$

One can then solve for the vector  $a^{(ij)}$  through  $a^{(ij)} = U^{-1}b^{(ij)}$  by applying the inverse matrix  $U^{-1}$ . The existence of  $U^{-1}$  implies the uniqueness of the solution for  $a^{(ij)}$ . An inverse problem is usually ill posed; namely, some elements of  $U^{-1}$  rise fast with its dimension. Nevertheless, the convergence of Eq. (15) can be achieved at a finite  $N$ , before  $U^{-1}$  goes out of control. The difference between an obtained solution and a true one produces a correction to Eq. (14) only at power  $1/u^{N+1}$ , and the coefficients  $a_n^{(ij)}$  built up previously are not altered by the inclusion of an additional higher-degree polynomial into the expansion in Eq. (15), because of the orthogonality condition in Eq. (16). The convergence of solutions in the polynomial expansion and their insensitivity to  $\Lambda$  will validate our approach, which is thus free of tunable parameters.

We get  $A_{ij}(s)$  from  $\Delta A_{ij}(s, \Lambda)$  by adding back the subtraction term, and the solution

$$y(s) = \frac{G_F^2 f_D^2 m_W^3 B_D}{12\pi^2 \Gamma} \sum_{i,j} \lambda_i \lambda_j \left\{ \Delta A_{ij}(s, \Lambda) + A_{ij}^{\text{box}}(s) \left[ 1 - e^{-(s-m_{IJ})^2/\Lambda^2} \right] \right\}, \quad (21)$$

in which only the components with  $m_{IJ} < m_D^2$  contribute to the physical value  $y(m_D^2)$ . In principle, one can evaluate  $x(s)$  by inserting Eq. (21) into Eq. (1). Note that the integration of the subtraction term to  $s \rightarrow \infty$  in Eq. (1) develops divergences, which ought to cancel in the summation over  $i, j$ . This delicate cancellation renders numerical outcomes unstable. A trick is to utilize the facts that the contributions to  $x(s)$  and  $y(s)$  from the box diagrams satisfy the dispersion relation in Eq. (10), and that they are four orders of magnitude smaller than our solutions as seen later. We then have

$$x(s) = \frac{G_F^2 f_D^2 m_W^3 B_D}{12\pi^3 \Gamma} \sum_{i,j} \lambda_i \lambda_j \left\{ \int_{m_{IJ}}^\infty \frac{ds'}{s-s'} \left[ \Delta A_{ij}(s', \Lambda) - A_{ij}^{\text{box}}(s') e^{-(s-m_{IJ})^2/\Lambda^2} \right] + \int_{m_{IJ}}^{m_{ij}} \frac{ds'}{s-s'} A_{ij}^{\text{box}}(s') \right\}, \quad (22)$$

where the integrals of  $A_{ij}^{\text{box}}(s')$  in the interval  $[m_{ij}, \infty)$  have been dropped in the light of the above argument. It is obvious that each term on the right-hand side of Eq. (22) is convergent. Our formalism can be extended to investigations of other neutral meson mixing straightforwardly with appropriate replacements of quark flavors, hadronic states, and the CKM matrix elements.

### III. D MESON MIXING

We first conduct the numerical analysis of the  $D$  meson mixing using the method developed in the previous section with the Fermi constant  $G_F = 1.1663788 \times 10^{-5} \text{ GeV}^{-2}$ , the decay constant  $f_D = 0.213 \text{ GeV}$ , the  $D$  meson decay

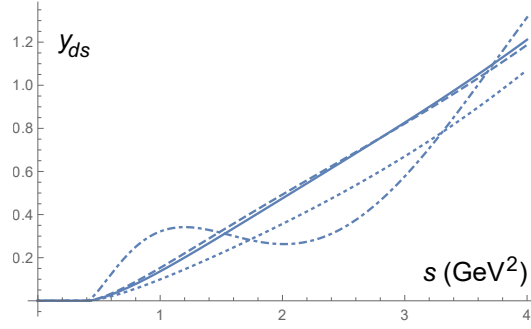


FIG. 2: Dependencies of  $y_{ds}(s) \equiv \Gamma_{ds}(s)/\Gamma$  on  $s$  for  $N = 3$  (dotted line),  $N = 8$  (dashed line),  $N = 13$  (solid line) and  $N = 23$  (dot-dashed line) with  $\Lambda = 5 \text{ GeV}^2$ .

width  $\Gamma = 1.60 \times 10^{-12} \text{ GeV}$  (corresponding to the lifetime  $\tau = 410.3 \times 10^{-15} \text{ s}$ ), the masses  $m_D = 1.865 \text{ GeV}$ ,  $m_d = 0.005 \text{ GeV}$ ,  $m_s = 0.093 \text{ GeV}$ ,  $m_b = 4.8 \text{ GeV}$  and  $m_W = 80.377 \text{ GeV}$ , the Wolfenstein parameters  $\lambda = 0.225$ ,  $A = 0.826$ ,  $\bar{\rho} = 0.159$  and  $\bar{\eta} = 0.348$  for the CKM matrix elements [47], and the typical bag parameter  $B_D \approx 1$ . The unitarity of the CKM matrix turns Eq. (5) for  $s = m_D^2$  into

$$\Gamma_{12}(m_D^2) = \lambda_s^2[\Gamma_{dd}(m_D^2) - 2\Gamma_{ds}(m_D^2) + \Gamma_{ss}(m_D^2)] + 2\lambda_s\lambda_b[\Gamma_{dd}(m_D^2) - \Gamma_{ds}(m_D^2)] + \lambda_b^2\Gamma_{dd}(m_D^2), \quad (23)$$

which indicates clearly that the charm mixing is sensitive to the flavor symmetry breaking. Substituting Eq. (6) from the box diagrams into the above expression, we find in the  $CP$ -conserving case, where only the real part of the CKM matrix element  $V_{ub}$  is considered, that the  $\lambda_s\lambda_b$  piece is positive with its magnitude being larger than of the negative  $\lambda_s^2$  piece. The  $\lambda_b^2$  piece, being of order of  $10^{-8}$ , is negligible compared with the first two, which are of order of  $10^{-7}$ . In total, the box diagrams contribute  $3.7 \times 10^{-7}$  to the parameter  $y$  for the  $D$  meson mixing, lower than the measured value by four orders of magnitude.

We solve for the component  $\Gamma_{ds}(s)$  in the decomposition of  $\Gamma_{12}(s)$  in Eq. (5) as a demonstration, computing the matrix  $U$  in Eq. (18) and the input vector  $b^{(ds)}$  in Eq. (20) for a given transition scale  $\Lambda$ , and deriving the unknown vector  $a^{(ds)} = U^{-1}b^{(ds)}$ . The dimension  $N$  of the matrix  $U$  is increased one by one to search for a convergent expansion in Eq. (15). When the convergence is attained, the solutions of  $a^{(ds)}$  and of  $\Delta A_{ds}(s, \Lambda)$  become stable with respect to the variation of  $N$ , which are then selected to form the solutions of  $\Gamma_{ds}(s)$  in Eq. (12). We list  $a_n^{(ds)}$  for  $\Lambda = 5 \text{ GeV}^2$  up to  $n = 23$  below,

$$\begin{aligned} & 10^5 \times (a_1^{(ds)}, a_2^{(ds)}, a_3^{(ds)}, \dots, a_{12}^{(ds)}, a_{13}^{(ds)}, a_{14}^{(ds)}, \dots, a_{22}^{(ds)}, a_{23}^{(ds)}) \\ & = (4.04, 2.47, 1.45, \dots, -2.08 \times 10^{-2}, -4.59 \times 10^{-3}, 9.25 \times 10^{-3}, \dots, 7.49 \times 10^{-2}, 1.04), \end{aligned} \quad (24)$$

whose magnitudes keep decreasing till  $n = 13$ , then increase with  $n$ , and  $a_{23}^{(ds)}$  becomes as large as the first few coefficients. The small ratio  $|a_{13}^{(ds)}/a_1^{(ds)}| \approx 10^{-3}$  marks a satisfactory convergence of the series up to  $n = 13$ , and the ill posed nature emerges gradually afterwards. We display the functions  $y_{ds}(s) \equiv \Gamma_{ds}(s)/\Gamma$  corresponding to  $N = 3, 8, 13$  and  $23$  for the expansion in Eq. (15) in Fig. 2. The dependencies on  $s$  match the pattern of Eq. (24): the curve of  $N = 3$  differs from those of  $N = 8$  and  $N = 13$ , which coincide with each other approximately. In fact, the curves for  $N$  around 13, including  $N = 11-15$ , overlap perfectly, confirming the convergence of the expansion in  $N$ . The curve of  $N = 23$  with obvious oscillations signals that the matrix elements of  $U^{-1}$  have gone out of control. The above examination suggests that  $N = 13$  is the optimal choice, and the corresponding  $y_{ds}(s)$  is the solution for the given  $\Lambda = 5 \text{ GeV}^2$ .

Repeating the steps, we determine the solutions of the components  $\Gamma_{dd}(s)$  and  $\Gamma_{ss}(s)$  with the optimal choices  $N = 16$  and  $N = 10$ , respectively, for the given  $\Lambda = 5 \text{ GeV}^2$ . The results of  $\Gamma_{ij}(s)$  are compared with the inputs  $\Gamma_{ij}^{\text{box}}(s)$  in terms of their ratios over the total width  $\Gamma$  in Fig. 3. It is seen that the solutions maintain the monotonic increase of the input functions with  $s$  basically, but the detailed behaviors have been modified by the physical thresholds. For  $y_{dd}^{\text{box}}(s) \equiv \Gamma_{dd}^{\text{box}}(s)/\Gamma$ , the hadron-level threshold  $4m_\pi^2$  and the quark-level threshold  $4m_d^2$  are both tiny, so the modification is minimal as shown in Fig. 3(a). The thresholds  $(m_\pi + m_K)^2$  and  $4m_K^2$  for  $y_{ds}$  and  $y_{ss} \equiv \Gamma_{ss}(s)/\Gamma$  at the hadron level are not only much greater than  $(m_d + m_s)^2$  and  $4m_s^2$  at the quark level, respectively, but sizable. Therefore, the difference between the solutions and the inputs is more salient, as exhibited in Figs. 3(b) and 3(c). The solutions stay vanishing till  $s$  crosses the physical thresholds, such that their magnitudes at higher  $s$  must be enhanced in order to compensate the loss at lower  $s$ , if the integral on the left-hand side of Eq. (11) remains equal

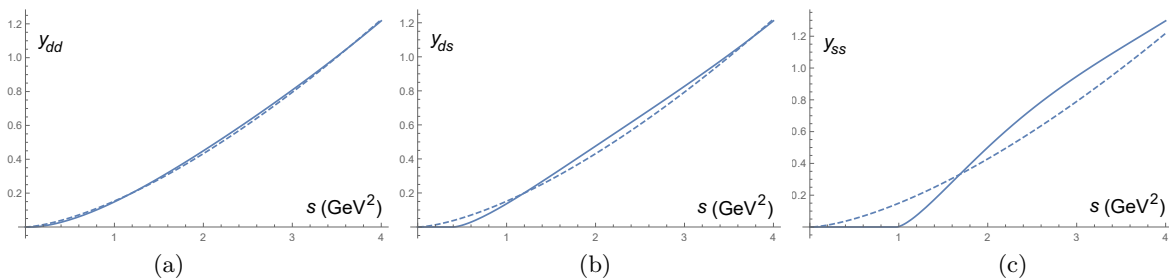


FIG. 3: Comparison of the solutions  $y_{ij}(s) \equiv \Gamma_{ij}(s)/\Gamma$  (solid lines) with the inputs  $y_{ij}^{\text{box}}(s) \equiv \Gamma_{ij}^{\text{box}}(s)/\Gamma$  (dashed lines) for (a)  $ij = dd$ , (b)  $ij = ds$  and (c)  $ij = ss$  at  $\Lambda = 5 \text{ GeV}^2$ .

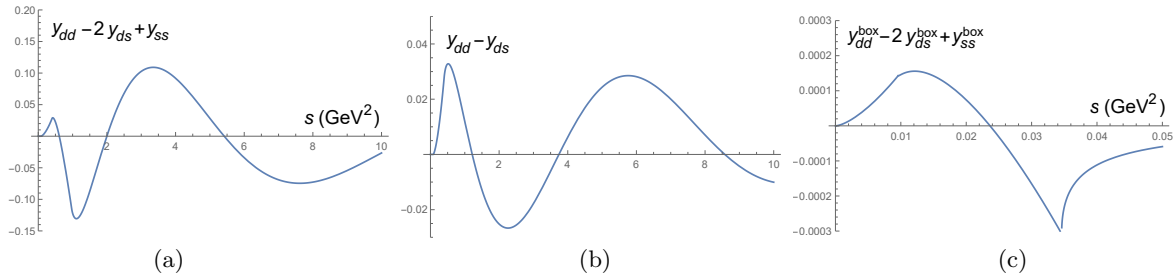


FIG. 4: Dependencies of (a)  $y_{dd} - 2y_{ds} + y_{ss}$ , (b)  $y_{dd} - y_{ds}$  and (c)  $y_{dd}^{\text{box}} - 2y_{ds}^{\text{box}} + y_{ss}^{\text{box}}$  on  $s$  for  $\Lambda = 5 \text{ GeV}^2$ .

to the right-hand side. This also explains why the enhancement is the most prominent in  $y_{ss}(s)$ , which is about 15% around the  $D$  meson mass squared  $s = m_D^2 \approx 3.5 \text{ GeV}^2$ , with the much larger threshold  $4m_K^2 \approx 1 \text{ GeV}^2$ . It is reasonable to claim 15% violation of the quark-hadron duality in the channel with two strange quarks for the  $D$  meson mixing, of the same order as postulated in [35]. All the solutions approach the inputs as  $s \rightarrow \infty$ , following the design in Eq. (12). The aforementioned modifications originate from the nonperturbative effects characterized by the physical thresholds  $m_{IJ} \neq m_{ij}$ , whose introduction for the components  $\Gamma_{ij}(s)$  in our formalism is unambiguous.

We present in Fig. 4 the dependencies of the combinations  $y_{dd} - 2y_{ds} + y_{ss}$  and  $y_{dd} - y_{ds}$  on  $s$ , which are associated with the CKM factors  $\lambda_s^2$  and  $\lambda_s \lambda_b$ , respectively, for the given  $\Lambda = 5 \text{ GeV}^2$ . The oscillations of the curve in Fig. 4(a) (not completely displayed in the plot) with the first peak (valley) located at  $s \approx (m_\pi + m_K)^2$  ( $s \approx 4m_K^2$ ) are anticipated [21]: when  $s$  increases and crosses the threshold  $(m_\pi + m_K)^2$  ( $4m_K^2$ ), the single (double) strange quark channel with a destructive (constructive) contribution is opened, so the curve starts to descend (ascend). It is not difficult to understand the minor oscillations at higher  $s$ , since heavier states stemming from the  $dd$ ,  $ds$  and  $ss$  channels are allowed to contribute in turn. These oscillations attenuate gradually, when the solutions for  $\Gamma_{dd}(s)$ ,  $\Gamma_{ds}(s)$  and  $\Gamma_{ss}(s)$  approach the perturbative inputs at large  $s$ , as indicated in Fig. 3, and the GIM suppression becomes effective. The curve for the combination  $y_{dd} - y_{ds}$  in Fig. 4(b) also reveals several oscillations but with smaller amplitudes, because of the stronger cancellation between  $y_{dd}$  and  $y_{ds}$  than between  $y_{ds}$  and  $y_{ss}$ . This pattern can be interpreted by means of Fig. 3, which shows the increasing enhancements from  $y_{dd}$  to  $y_{ds}$  and to  $y_{ss}$  at  $s = m_D^2$  compared with the inputs. Hence, the SU(3) symmetry breaking between the first two is smaller than between the last two. The first peak in Fig. 4(b) appears at  $s \approx (m_\pi + m_K)^2$  as expected, but the other peaks and valleys are shifted toward slightly higher  $s$  compared to Fig. 4(a): the constructive  $ss$  channel is absent, so the descent of the curve cannot be reversed at  $s \approx 4m_K^2$ .

The aforementioned combinations of  $y_{ij}$ , where the box-diagram terms in Eq. (12) cancel almost exactly, are in fact proportional to those of the subtracted functions  $\Delta\Gamma_{ij}$ . The results in Figs. 4(a) and 4(b), multiplied by the corresponding CKM factors  $\lambda_s^2$  and  $2\lambda_s \lambda_b$ , respectively, then behave differently from the box-diagram contributions: both pieces from the box diagrams are of  $O(10^{-7})$  at the  $D$  meson mass, but the  $\lambda_s^2$  piece in our solutions becomes  $O(10^{-3})$ , and dominant over the  $\lambda_s \lambda_b$  piece, which is of  $O(10^{-6})$ . The smallness of the latter is not only attributed to the shorter peak of  $y_{dd} - y_{ds}$ , but to its shift away from the  $D$  meson mass, as shown in Fig. 4(b). The  $\lambda_b^2$  piece, depending on  $y_{dd}$  in Fig. 3(a), is as tiny as  $O(10^{-7})$ . The SU(3) symmetry breaking effects from the various thresholds  $m_{IJ}$ , i.e., various enhancements in Figs. 3(a)-3(c), are manifested by the dramatically different magnitudes of the combination  $y_{dd} - 2y_{ds} + y_{ss}$  in Fig. 4(a) and of  $y_{dd}^{\text{box}} - 2y_{ds}^{\text{box}} + y_{ss}^{\text{box}}$  in Fig. 4(c). Another feature of Fig. 4(c) is that the shape of the curve is trivial: it reaches a peak at  $s \approx (m_d + m_s)^2$  and a valley at  $s \approx 4m_s^2$ , and then



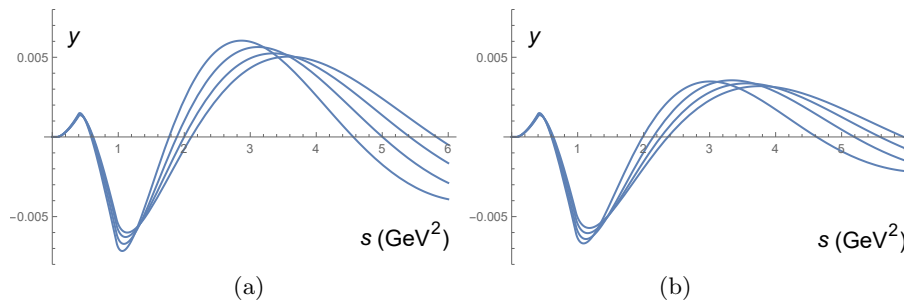


FIG. 5: Solutions of  $y(s)$  for  $\Lambda = 4.0 \text{ GeV}^2$ ,  $4.5 \text{ GeV}^2$ ,  $5.0 \text{ GeV}^2$  and  $5.5 \text{ GeV}^2$ , corresponding to the curves with the peaks from left to right, in the cases (a) with and (b) without the second term in Eq. (20).

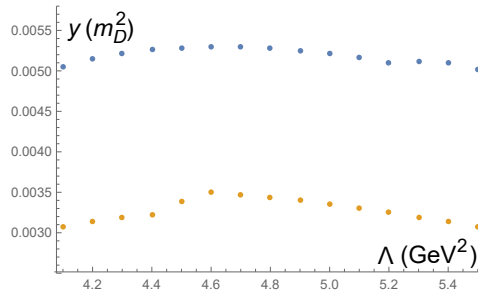


FIG. 6: Dependencies of  $y(m_D^2)$  on  $\Lambda$  in the cases with (upper curve) and without (lower curve) the second term in Eq. (20).

approaches zero smoothly.

We then investigate how the solutions for the mixing parameter  $y(s)$  change with the transition scale  $\Lambda$ , starting from the CP-conserving case. The contributions from all the three pieces  $\lambda_s^2$ ,  $\lambda_s\lambda_b$  and  $\lambda_b^2$  are included, though the behavior of  $y(s)$  is governed by the first piece as stated above. It is encouraging to see in Fig. 5(a) that the curves for  $\Lambda = 4.0 \text{ GeV}^2$ ,  $4.5 \text{ GeV}^2$ ,  $5.0 \text{ GeV}^2$  and  $5.5 \text{ GeV}^2$  all pass through the small region around  $s \approx m_D^2$  and  $y \approx 0.5\%$ . Namely, a stability window in  $\Lambda$  may exist, within which the obtained  $y(m_D^2)$  is insensitive to  $\Lambda$ . The tails of these curves are far apart from each other, implying that they will not cross again at higher  $s$ . Therefore,  $y(m_D^2) \approx 0.5\%$  is the unique solution from our method. Note that the above curves overlap completely in the region with  $s < 1 \text{ GeV}^2$ , which, however, do not represent solutions for the physical  $D$  meson apparently. To verify the postulation that the nonperturbative effects from the physical thresholds are crucial for stabilizing the solutions, we drop the second term in the input in Eq. (20), and derive  $y(s)$  for the same set of  $\Lambda$  values in Fig. 5(b). The curves have shapes similar to those in Fig. 5(a), but scatter to some degree, such that the area in which they cross each other stretches. It means that the stability deteriorates in the absence of the nonperturbative effects. Besides, the magnitudes at  $s \approx m_D^2$  reduce by about 40%, which is the appropriate weight of nonperturbative contributions to achieve the stability in QCD sum rules.

We read off the values of  $y(m_D^2)$  at the  $D$  meson mass squared  $s = m_D^2$  from the curves like those in Fig. 5, and plot the dependencies of  $y(m_D^2)$  on the transition scale  $\Lambda$  in the cases with and without the second term in Eq. (20). It is noticed in Fig. 6 that the former ascends with  $\Lambda$  first, reaches a plateau around  $\Lambda = 4.5 \text{ GeV}^2$ , and then descends as  $s > 4.8 \text{ GeV}^2$ . Selecting the values in the range  $\Lambda = [4.2, 5.1] \text{ GeV}^2$  as our representative results, we have  $y(m_D^2) = (0.52 \pm 0.01)\%$ , where the central value is located at  $\Lambda = 4.3 \text{ GeV}^2$ , and the tiny error reflects the remarkable stability of  $y(m_D^2)$  with respect to the variation of  $\Lambda$ . For  $s$  slightly below (above)  $m_D^2$ , say,  $s = 3.0 \text{ GeV}^2$  ( $s = 4.0 \text{ GeV}^2$ ), Fig. 5(a) indicates that  $y$  always decreases (increases) with  $\Lambda$ . The obtained  $y(m_D^2)$ , greater than in the exclusive analysis focusing only on two-body decays [18], hints the sizable contributions from the resonances or multi-body states near the  $D$  meson mass [7, 18, 48]. As the nonperturbative effects are ignored, the plateau in  $\Lambda$  disappears: the curve ascends with  $\Lambda$ , and then descends from the maximum located at  $\Lambda = 4.6 \text{ GeV}^2$  directly, such that it is hard to extract any physical outcomes in this case. We stress that there is no free parameter in our approach, which can be tuned to achieve data fitting. The solutions of  $y(m_D^2)$  are insensitive to the number  $N$  for the polynomial expansion and to the arbitrary transition scale  $\Lambda$  as stated before. We mention that the renormalization scales associated with the different channels for  $y$  in the heavy quark expansion took different values so as to accommodate the data by avoiding the stringent GIM cancellation [49].

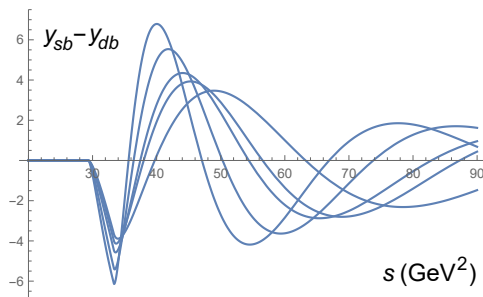


FIG. 7: Behaviors of  $y_{sb} - y_{db} \equiv (\Gamma_{sb} - \Gamma_{db})/\Gamma$  for  $\Lambda = 15 \text{ GeV}^2, 20 \text{ GeV}^2, 25 \text{ GeV}^2, 30 \text{ GeV}^2$  and  $35 \text{ GeV}^2$ , corresponding to the curves with the peaks from left to right.

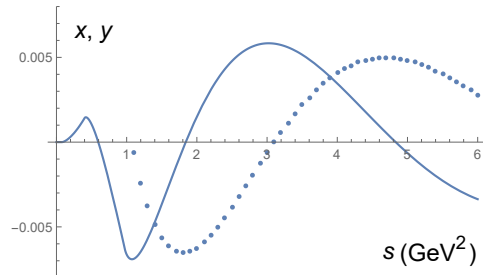


FIG. 8: Behaviors of  $x(s)$  (dotted line) and  $y(s)$  (solid line) for  $\Lambda = 4.3 \text{ GeV}^2$ .

We then calculate the mixing parameter  $x(m_D^2)$  according to Eq. (22), for which the other three components involving  $b$  quarks, i.e.,  $\Gamma_{db}(s)$ ,  $\Gamma_{sb}(s)$  and  $\Gamma_{bb}(s)$  should be available first. Similarly, we seek the most convergent solutions in the polynomial expansion with the same power-law behaviors near the physical thresholds for the above three components. The dependences of the combination  $y_{sb} - y_{db} \equiv (\Gamma_{sb} - \Gamma_{db})/\Gamma$  on  $s$  for  $\Lambda = 15 \text{ GeV}^2, 20 \text{ GeV}^2, 25 \text{ GeV}^2, 30 \text{ GeV}^2$  and  $35 \text{ GeV}^2$  are displayed in Fig. 7. The curves run along the horizontal axis till the threshold near  $m_D^2$  (the pion and kaon masses can be ignored here), and then oscillate, similar to the curves in Fig. 4. It is seen that the curves corresponding to  $\Lambda = 25 \text{ GeV}^2$  and  $30 \text{ GeV}^2$  are relatively close to each other, revealing sort of stability. Since the result of  $x(m_D^2)$  has little dependence on these components, which take substantial values at  $s$  far away from  $m_D^2$ , we simply fix  $\Lambda$  to  $30 \text{ GeV}^2$ , with which  $N = 10$  ( $N = 11$ ) is chosen for  $\Gamma_{db}(s)$  ( $\Gamma_{sb}(s)$ ). The contribution to  $x(m_D^2)$  from the component  $\Gamma_{bb}(s)$  is even less important, so we also set  $\Lambda = 30 \text{ GeV}^2$  for its evaluation for simplicity. It turns out that the contributions from the above three components to  $x(m_D^2)$  via Eq. (22) are as low as  $2.2 \times 10^{-7}$ , among which  $\Gamma_{bb}(s)$ , contributing  $O(10^{-10})$ , is absolutely negligible.

The curve of  $y(s)$  for  $\Lambda = 4.3 \text{ GeV}^2$ , which gives rise to the central value of  $y(m_D^2)$ , together with the corresponding  $x(s)$  derived from Eq. (22), are exhibited in Fig. 8, from which we read off the central value  $x(m_D^2) = 0.21\%$ . The correlation between  $x(s)$  and  $y(s)$  is similar to what was observed in [21]. The lower (upper) bound of  $y(m_D^2)$  located at  $\Lambda = 4.2$  ( $\Lambda = 4.5$ )  $\text{GeV}^2$  leads to the upper (lower) bound of  $x(m_D^2) = 0.24\%$  ( $0.15\%$ ). That is, we obtain  $x(m_D^2) = (0.21^{+0.03}_{-0.06})\%$ , whose error reflects the uncertainty in our method. We then survey the uncertainties from the theoretical inputs. The parameters involved in the CKM matrix and the hadron masses have been known precisely, so the associated uncertainties are minor. It has been affirmed that our results are insensitive to the down quark mass  $m_d$ , and the  $\pm 10\%$  variation of the strange quark mass  $m_s$  induces only  $\mp 0.6\%$  error to the value of  $y(m_D^2)$ . The uncertainty from the overall hadronic parameters, like the bag parameters, is about 5% according to [44, 50]. We present our predictions for the mixing parameters in the  $CP$ -conserving case, including the overall 5% uncertainty, as

$$x(m_D^2) = (0.21^{+0.04}_{-0.07})\%, \quad y(m_D^2) = (0.52 \pm 0.03)\%. \quad (25)$$

It is emphasized that the uncertainties from neglected subleading contributions to the inputs at large mass have not been taken into account. According to [32], the  $O(\alpha_s)$  and  $O(1/m_b)$  corrections,  $\alpha_s$  being the strong coupling constant, amount to about 20% of the leading contribution to the  $B_s$  meson width difference. It is thus likely that the results in Eq. (25) suffer additional uncertainties of order 20%.

It has been shown in lattice analyses [51] that the  $(S-P)(S-P)$  hadronic matrix element for the  $D$  meson mixing is larger than the  $(V-A)(V-A)$  one. This observation is understandable, because the former is proportional to

an additional factor  $m_D^2/(m_c + m_u)^2 \approx 2$  actually,  $m_u$  being the  $u$  quark mass. Therefore, it is possible to gain an overall 30% enhancement of our predictions by considering the above factor, which then agree with the data [1]

$$x = (0.44_{-0.15}^{+0.13})\%, \quad y = (0.63 \pm 0.07)\%, \quad (26)$$

in the  $CP$ -conserving case. Our goal is not to achieve an exact fit to the data, but to demonstrate that the box-diagram contribution to the  $D$  meson mixing can be amplified by a factor of  $10^4$  under the nonperturbative  $SU(3)$  breaking effects. A precise study can be carried out by employing the weak effective Hamiltonian and the hadronic matrix elements with higher accuracy for the perturbative inputs in our formalism.

The  $CP$  violation in the  $D$  meson mixing has been discussed and formulated in detail in [52]. In the  $CP$  violating case we simply multiply our solution for each component  $\Gamma_{ij}$  in Eq. (5) by the associated complex CKM factors, and both  $M_{12}$  and  $\Gamma_{12}$  become complex. We then adopt the general definitions of the mixing parameters  $x$  and  $y$  in Eq. (3), and find that the imaginary parts of  $M_{12}$  and  $\Gamma_{12}$ , being of  $Q(10^{-3})$  and  $O(10^{-4})$  of the real parts, respectively, are negligible. Hence, our predictions for  $x$  and  $y$  remain the same as in Eq. (25) basically, and will be close to the data

$$x = (0.409_{-0.049}^{+0.048})\%, \quad y = (0.615_{-0.055}^{+0.056})\%, \quad (27)$$

in the  $CP$ -violating case [1], after the enhancement from the  $(S - P)(S - P)$  hadronic matrix element is taken into account. We also derive

$$\left| \frac{q}{p} \right| - 1 = (-3.0_{-0.0}^{+0.1}) \times 10^{-4}, \quad \text{Arg} \left( \frac{q}{p} \right) = (3.1_{+0.4}^{-0.3})^\circ \times 10^{-3}, \quad (28)$$

where the central values (the upper errors, the lower errors) come from the scales  $\Lambda = 4.3 \text{ GeV}^2$  ( $\Lambda = 4.2 \text{ GeV}^2$ ,  $\Lambda = 4.5 \text{ GeV}^2$ ). They can be compared with the measured values  $|q/p| = 0.995 \pm 0.016$  and  $\text{Arg}(q/p) = (-2.5 \pm 1.2)^\circ$  [1], which were obtained under the same phase convention for the  $CP$  transformation of neutral  $D$  mesons, and help constrain new physics models [53, 54] due to their small theoretical uncertainties. Besides, we predict the quantity  $\phi_{12} \equiv \text{Arg}(M_{12}/\Gamma_{12}) \approx -0.049^\circ$  in accordance with the data  $\phi_{12} = (0.58_{-0.90}^{+0.91})^\circ$  [1].

#### IV. $B_{s(d)}$ MESON MIXING AND KAON MIXING

Tremendous efforts have been devoted to perturbative studies of the  $B_{d(s)}$  meson mixing and the kaon mixing, and to their confrontation with data in the literature. The transition matrix elements  $M_{12}^{s(d)} - i\Gamma_{12}^{s(d)}/2$  for the  $B_{d(s)}$  meson mixing have been evaluated up to two-loop QCD corrections in the heavy quark expansion [55, 56]. The ratio of the width difference over the mass difference,  $\Delta\Gamma_{s(d)}/\Delta M_{s(d)} = \text{Re}(\Gamma_{12}^{s(d)}/M_{12}^{s(d)})$ , where hadronic uncertainties largely cancel, was computed in [56]. The experimental input  $\Delta M_{s(d)}^{\text{exp}}$  was then inserted to predict  $\Delta\Gamma_{s(d)}$ , which was shown to be consistent with the data. It implies that the  $B_{s(d)}$  meson mixing can be accommodated by short-distance dynamics within hadronic uncertainties. A similar conclusion on the dominance of short-distance dynamics in the measured kaon mass difference was also drawn [38–40]. Therefore, we do not attempt precise explanations of the  $B_{s(d)}$  meson mixing and the kaon mixing in this paper, on which a lot of progresses have been made, but corroborate that the neutral meson mixing, no matter whether it is governed by perturbative or nonperturbative dynamics, can be addressed consistently and systematically in our framework.

We decompose the absorptive piece of the transition matrix elements for the  $B_{s(d)}$  meson mixing into

$$\Gamma_{12}^{s(d)}(m_{B_{s(d)}}^2) = \lambda_u^{s(d)2}\Gamma_{uu}^{s(d)}(m_{B_{s(d)}}^2) + 2\lambda_u^{s(d)}\lambda_c^{s(d)}\Gamma_{uc}^{s(d)}(m_{B_{s(d)}}^2) + \lambda_c^{s(d)2}\Gamma_{cc}^{s(d)}(m_{B_{s(d)}}^2), \quad (29)$$

to which a top quark does not contribute, with the CKM factors  $\lambda_u^{s(d)} = V_{ub}V_{us(d)}^*$  and  $\lambda_c^{s(d)} = V_{cb}V_{cs(d)}^*$ , and the meson mass  $m_{B_d}$ . The box-diagram contributions  $\Gamma_{ij}^{s(d)\text{box}}(s)$  are the same as Eq. (6), but with the replacements of  $f_D$  ( $m_D$ ,  $B_D$ ) by  $f_{B_{d(s)}}$  ( $m_{B_{d(s)}}$ ,  $B_{B_{d(s)}}$ ), and of  $m_d$  ( $m_s$ ) by  $m_u$  ( $m_c$ ). They yield the width difference  $\Delta\Gamma_s = 0.099 \text{ ps}^{-1}$  from Eq. (29) for the  $B_s$  meson mass (decay constant)  $m_{B_s} = 5.367 \text{ GeV}$  ( $f_{B_s} = 0.230 \text{ GeV}$ ) [47], the quark masses  $m_u = 0.005 \text{ GeV}$  and  $m_c = 1.3 \text{ GeV}$ , and the typical bag parameter  $B_{B_s} = 1$ , close to the observed value  $\Delta\Gamma_s^{\text{exp}} = (0.084 \pm 0.005) \text{ ps}^{-1}$  [1] as stated above. The components  $\Gamma_{uu}^{s(d)}(s)$ ,  $\Gamma_{uc}^{s(d)}(s)$  and  $\Gamma_{cc}^{s(d)}(s)$  for a fictitious  $B_{s(d)}$  meson with the invariant mass squared  $s$  will be derived in our method. The solutions for the  $B_s$  and  $B_d$  mesons are expected to be very similar, so the distinction between  $\Gamma_{12}^s(s)$  and  $\Gamma_{12}^d(s)$  mainly comes from the CKM factors. Because of the hierarchy  $|\lambda_u^s| \ll \lambda_c^s$ , no cancellation occurs among the three pieces in Eq. (29), such that the last term dominates  $\Gamma_{12}^s(m_{B_s}^2)$ , as having been noticed in [57]. As to the  $B_d$  meson mixing, for which  $|\lambda_u^d|$  and  $|\lambda_c^d|$  are of the

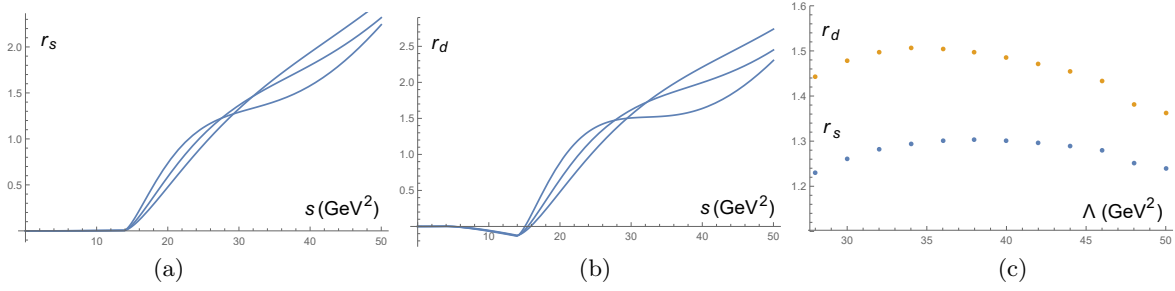


FIG. 9: Solutions of (a)  $r_s(s)$  and (b)  $r_d(s)$  for  $\Lambda = 30 \text{ GeV}^2$ ,  $40 \text{ GeV}^2$  and  $50 \text{ GeV}^2$ , corresponding to the curves which rise at the threshold  $s = 4m_D^2$  from left to right. (c) Dependencies of  $r_s(m_{B_s}^2)$  and  $r_d(m_{B_d}^2)$  on  $\Lambda$ .

same order of magnitude but unequal, a milder cancellation exists, and all the three pieces in Eq. (29) contribute to  $\Gamma_{12}^d(m_{B_d}^2)$ .

The construction of the dispersion relation for the  $B_{d(s)}$  meson mixing follows the steps in Sec. II, and the aforementioned  $\Gamma_{ij}^{s(d)\text{box}}(s)$  from the box diagrams are taken as the inputs. We solve for the unknown vector  $a^{(ij)}$  with the input vector  $b^{(ij)}$  in Eq. (20) to get the components  $\Gamma_{uu}^{s(d)}(s)$ ,  $\Gamma_{uc}^{s(d)}(s)$  and  $\Gamma_{cc}^{s(d)}(s)$  for various transition scales  $\Lambda$  as in the previous section. Here we consider the ratio

$$r_{s(d)}(s) \equiv \frac{\Gamma_{12}^{s(d)}(s)}{\Gamma_{12}^{s(d)\text{box}}(m_{B_{s(d)}}^2)}, \quad (30)$$

which is free of the hadronic uncertainties from the decay constant  $f_{B_{d(s)}}$  and the bag parameters  $B_{B_{d(s)}}$ . It will be seen that there are stable solutions of order of unity for the ratio  $r_{s(d)}(m_{B_{s(d)}}^2)$ . In other words, the obtained  $B_{s(d)}$  meson width difference does not deviate from the box-diagram contribution much under the nonperturbative effects. We mention that the quark-hadron duality, i.e., the equivalence between the quark-level and hadron-level evaluations of the  $B_s$  meson width difference, has been demonstrated in [58].

We focus only on the  $CP$ -conserving case by picking up the real part of the CKM matrix element  $V_{ub}$ , and adopt the quark masses  $m_u = 0.005 \text{ GeV}$  and  $m_c = 1.3 \text{ GeV}$ , and the meson masses  $m_{B_s} = 5.369 \text{ GeV}$  and  $m_{B_d} = 5.280 \text{ GeV}$  [47]. The best convergence of the polynomial expansion associated with the component  $\Gamma_{uu}^{s(d)}(s)$  ( $\Gamma_{uc}^{s(d)}(s)$ ,  $\Gamma_{cc}^{s(d)}(s)$ ) fixes the optimal numbers  $N = 16, 16$  and  $16$  ( $N = 14, 15$  and  $15$ ,  $N = 11, 11$  and  $10$ ) for  $\Lambda = 30 \text{ GeV}^2$ ,  $40 \text{ GeV}^2$  and  $50 \text{ GeV}^2$ , respectively. It is encouraging to find that the three curves of  $r_s$  ( $r_d$ ) for the above  $\Lambda$  values cross each other in the small region around  $s \approx m_{B_{s(d)}}^2$  and  $r_s \approx 1.3$  ( $r_d \approx 1.5$ ) in Fig. 9(a) (Fig. 9(b)). Namely, a stability window in  $\Lambda$  is present, within which the solutions of  $r_{s(d)}(m_{B_{s(d)}}^2)$  are insensitive to  $\Lambda$ . This feature is similar to that of  $y(m_D^2)$  in Fig. 6. Since all the three pieces on the right-hand side of Eq. (29) contribute to  $r_d(s)$ , it does not vanish below the threshold  $s = 4m_D^2$  as displayed in Fig. 9(b). Moreover, the width difference for the  $B_d$  meson is about  $\lambda^2 \sim 0.05$  of the  $B_s$  meson one in agreement with the data [1].

We read off the values of  $r_{s(d)}(m_{B_{s(d)}}^2)$ , and plot its dependence on the scale  $\Lambda$  in Fig. 9(c). It is noticed that the curve for  $r_{s(d)}(m_{B_{s(d)}}^2)$  ascends with  $\Lambda$  first, becomes relatively flat around  $\Lambda = 38 \text{ GeV}^2$  ( $\Lambda = 34 \text{ GeV}^2$ ), where the maximum is located, and then descends monotonically. Selecting the values in the intervals  $\Lambda = [32, 46] \text{ GeV}^2$  and  $\Lambda = [30, 42] \text{ GeV}^2$  as our representative results, we have

$$r_s(m_{B_s}^2) = 1.29 \pm 0.01, \quad r_d(m_{B_d}^2) = 1.49 \pm 0.02, \quad (31)$$

respectively, whose tiny errors reflect the excellent stability of our solutions in the wide ranges of  $\Lambda$ . The solution for  $\Gamma_{12}^s(m_{B_s}^2)$  is indeed of the same order as the input  $\Gamma_{12}^{s\text{box}}(m_{B_s}^2)$ , as indicated by Eq. (31). The value  $r_d(m_{B_d}^2)$  is slightly larger owing to the partial cancellation among the perturbative contributions to the three pieces in Eq. (29). The above investigation confirms that the nonperturbative effects associated with the physical thresholds do not impact much the width differences, the quark-hadron duality holds reasonably well for the  $B_{s(d)}$  meson mixing, and short-distance dynamics dominates the relevant observables.

The absorptive piece  $\Gamma_{12}^K(s)$  for a fictitious kaon with the invariant mass squared  $s$  is also decomposed in terms of the CKM factors  $\lambda_k \equiv V_{ks}V_{kd}^*$ ,  $k = u, c, t$ . Only the component  $\Gamma_{uu}^K(m_K^2)$  contributes to  $\Gamma_{12}^K(m_K^2)$ , because a kaon does not decay into final states with charm quarks. The expression of the corresponding input  $\Gamma_{uu}^{K\text{box}}(s)$  at large  $s$  is the same as Eq. (6), but with the appropriate replacements of the decay constant, the particle masses, and the bag parameter.

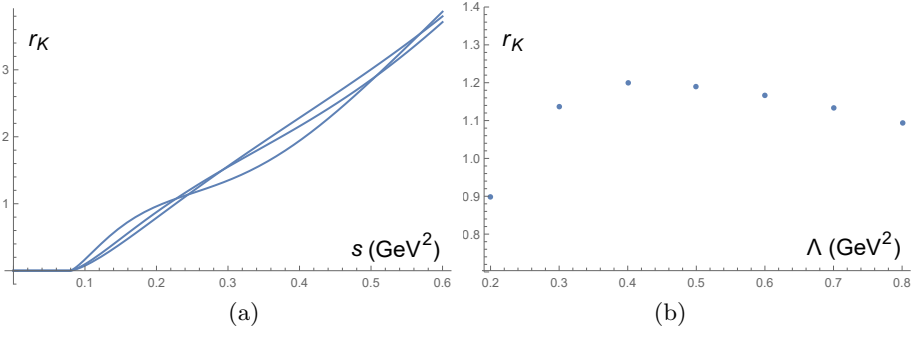


FIG. 10: (a) Solutions of  $r_K(s)$  for  $\Lambda = 0.3 \text{ GeV}^2$ ,  $0.5 \text{ GeV}^2$  and  $0.7 \text{ GeV}^2$ , corresponding to the curves which rise from the threshold  $s = 4m_\pi^2$  from left to right. (b) Dependence of  $r_K(m_K^2)$  on  $\Lambda$ .

Note that the  $CP$  transformation sets  $CP|D^0\rangle = -|\bar{D}^0\rangle$  in Sec. II, so  $K_1$  ( $K_2$ ) refers to  $K_L$  ( $K_S$ ) in the analogous convention. The width difference is almost equal to the width of  $K_S$ , i.e.,  $\Gamma_2^K - \Gamma_1^K = 2\Gamma_{12}^K \approx \Gamma_2^K = 7.347 \times 10^{-15} \text{ GeV}$  in experiments [47]. It is straightforward to check that the box-diagram contribution is lower, but accounts for the measured width difference at the order of magnitude. The higher-order QCD corrections to the effective weak Hamiltonian [59] and the penguin contribution [60] can be included into the input for a more precise analysis. Here we simply calculate the ratio

$$r_K(s) \equiv \frac{\Gamma_{12}^K(s)}{\Gamma_{12}^{K\text{box}}(m_K^2)}, \quad (32)$$

with the denominator being derived from the box diagrams, and examine whether the ratio is of order of unity.

We solve for the component  $\Gamma_{uu}^K(s)$  for various scales  $\Lambda$  by repeating the procedures, and search for stable solutions of  $r_K(m_K^2)$ . The best convergence of the polynomial expansion associated with  $\Gamma_{uu}^K(s)$  determines the numbers  $N = 11$ , 10 and 12 for  $\Lambda = 0.3 \text{ GeV}^2$ ,  $0.5 \text{ GeV}^2$  and  $0.7 \text{ GeV}^2$ , respectively. The corresponding results of  $r_K(s)$  are exhibited in Fig. 10(a), whose curves cross each other in the small region around  $s \approx m_K^2$  and  $r_K \approx 1.2$ . That is, a stability window in  $\Lambda$  can be identified, within which  $r_K(m_K^2)$  is insensitive to  $\Lambda$ . We acquire the solutions for  $r_K(s)$ , read off the values of  $r_K(m_K^2)$ , and present its dependence on  $\Lambda$  in Fig. 10(b). The curve, with the shape similar to that of  $r_{s(d)}(m_{B_{s(d)}}^2)$  in Fig. 9(c), is relatively flat around  $\Lambda = 0.4 \text{ GeV}^2$ . Selecting  $r_K(m_K^2)$  in the interval  $\Lambda = [0.3, 0.7] \text{ GeV}^2$  as our representative results, we get

$$r_K(m_K^2) = 1.17 \pm 0.03, \quad (33)$$

which, close to unity, hints the importance of short-distance contributions in the kaon mixing. We point out that the scale  $\Lambda$  also bears the meaning of a resolution power of the inverse matrix method [28], so  $\Lambda$  takes values near the resonance to be explored. It is then realized why the stability window appears at  $\Lambda$  about hundreds of  $\text{MeV}^2$ , few  $\text{GeV}^2$  and tens of  $\text{GeV}^2$  in the kaon mixing, the  $D$  meson mixing and the  $B_{s(d)}$  meson mixing, respectively.

At last, we summarize our observations on the neutral meson mixing mechanism, and highlight the uniqueness of the charm mixing. For a more transparent illustration, we reexpress the absorptive piece of the transition matrix elements for the charm mixing as

$$\Gamma_{12}(m_D^2) = \lambda_d^2 \Gamma_{dd}(m_D^2) + 2\lambda_d \lambda_s \Gamma_{ds}(m_D^2) + \lambda_s^2 \Gamma_{ss}(m_D^2), \quad (34)$$

which turns the cancellation among the decay channels in Eq. (23) into the cancellation among the components associated with the three CKM factors, because of the relation  $\lambda_d^2 \approx -\lambda_d \lambda_s \approx \lambda_s^2$ . In fact, at most 15% duality violation for each component in the  $D$  meson mixing is less severe than in the others given in Eqs. (31) and (33). Comparing  $2m_K$  with  $m_D$  and  $2m_D$  with  $m_{B_s}$ , we see that the physical threshold is further below the neutral meson mass in the  $D$  meson mixing than in the  $B_s$  meson mixing. It is the reason why the deviation of the solution from the perturbative input caused by the threshold is minor in the former. As shown in [61], the charm width difference receives corrections from next-to-leading order QCD below 50%, and  $1/m_c$  corrections of 30%. That is, subleading contributions in the charm mixing do not reveal signs of breakdown of the perturbative approach. Besides, the lifetime ratio  $\tau(D^+)/\tau(D^0)$ , which is insensitive to  $SU(3)$  breaking and not subject to the GIM suppression, agrees with the data [47], as calculated up to leading order in the  $1/m_c$  expansion based on the formulation in [62]. Therefore, it is the GIM cancellation in Eq. (34) which strongly suppresses the perturbative contributions, and fails the inclusive analyses.

It has been known that such cancellation does not take place in the  $B_{s(d)}$  meson mixing, since the CKM factors in Eq. (29) do not follow the pattern in the charm mixing. The CKM factors for the kaon mixing obey the similar pattern,  $\lambda_u^2 \approx -\lambda_u \lambda_c \approx \lambda_c^2$ . However, only the first piece associated with  $\lambda_u^2$  survives the phase space constraint, so the delicate cancellation does not happen either. Without the GIM cancellation, short-distance dynamics remains important in the  $B_{s(d)}$  meson mixing and the kaon mixing.

## V. CONCLUSION

We have analyzed the neutral meson mixing in the framework based on the dispersion relation, from which the width difference of the two neutral meson mass eigenstates is solved directly. The idea is to treat the dispersion relation as an inverse problem, in which nonperturbative observables at low mass are solved with perturbative inputs from high mass. It was emphasized that initial conditions of solutions at physical thresholds for involved decay channels play an essential role. Their distinctions from the thresholds at the quark level provide the nonperturbative effects, which determine how significantly the solution for each channel deviates from the corresponding perturbative input. The physical thresholds for various channels induce the SU(3) symmetry breaking, which is the key to explain the  $D$  meson mixing. The threshold-dependent contributions, acting like nonperturbative power corrections in QCD sum rules, also stabilize the results of the mixing parameter  $y(s = m_D^2)$  in the inverse problem: the convergence of the solutions in the polynomial expansion and the insensitivity to the arbitrary transition scale, which was introduced through the ultraviolet regularization of the dispersive integrals, have been demonstrated. In this sense, our formalism is free of tunable parameters, and this work represents an improvement of our previous one, which relies on a discretionary parametrization for the mixing parameter  $y(s)$ .

It is intriguing to find that the solutions of  $y(s)$  exhibit several oscillations, which reflect the alternate opening of the destructive and constructive channels with the increase of the phase space. The peak of the function  $y(s)$  around the  $D$  meson mass with the height greater than in the previous exclusive analyses based only on two-body modes suggests that nearby resonances or multi-particle decays give the sizable contributions to  $y(m_D^2)$ . The channel with two strange quarks, i.e., di-kaon states, provides the major source of the SU(3) breaking relative to the channels with two down quarks and with one down quark and one strange quark, which enhances the net contribution to  $y(m_D^2)$  by four orders of magnitude compared with the perturbative inputs. The mixing parameter  $x(m_D^2)$  was derived from the dispersive integration of  $y(s)$ , to which the contributions from the three channels containing  $b$  quarks are negligible. The solutions for the various channels can be employed to calculate the mixing parameters in both the  $CP$ -conserving and  $CP$ -violating cases: we simply multiply the solutions by the associated CKM factors without and with the imaginary parts, respectively. It has been argued that our results for  $x(m_D^2)$  and  $y(m_D^2)$  can accommodate the data, after the enhancement from the matrix element of the  $(S - P)(S - P)$  effective operator is taken into account. The theoretical uncertainty in our method is controllable, reflected by the very flat plateau of  $y(m_D^2)$  in the stability window of  $\Lambda$ . In addition, we have predicted the coefficient ratio  $q/p$  in the  $CP$ -violating case, which can be scrutinized by future precise measurements.

We have also studied the  $B_{s(d)}$  meson mixing and the kaon mixing in the same framework. It was found that the deviation of the solution from the corresponding perturbative input is at the  $O(10\%)$  level for each channel in the width difference, and the breakdown of the quark-hadron duality is similar to the amount in the charm mixing. Because there exists no or milder cancellation of the perturbative pieces among the different channels, short-distance dynamics can be relatively important. Hence, the duality violation is not the major cause that renders the  $D$  meson mixing special from the others. It is the GIM cancellation that makes the tiny perturbative contributions in the inclusive analyses, in contrast to which the SU(3) breaking effects manifest in the  $D$  meson mixing. We stress that our work does not aim at a precise calculation and an exact match to the data, but at the verification that the box-diagram contributions can be greatly enhanced to the order of magnitude of the observed charm mixing, and the neutral meson mixing, no matter whether it is governed by perturbative or nonperturbative dynamics, can be addressed consistently and systematically in our formalism.

To improve the precision of the predictions, more accurate hadronic matrix elements of the effective operators, available higher-order corrections to the effective weak Hamiltonian [63, 64], subleading contributions from heavy quarks [65], and corrections with amplitudes being topologically distinct from the box diagrams, like the double penguin contribution [66], can be included into the inputs of our method. Simply speaking, the ultimate precision of the results is controlled by the accuracy of the inputs at large mass, i.e., of our understanding on the  $B$  meson mixing. It is then promising to lower the uncertainties down to 10% level [64]. A thorough picture of the neutral meson mixing mechanism will help explorations of other observables, such as effects of the  $D$  meson mixing in the extraction of the weak phase  $\gamma$  from the  $B \rightarrow DK$  decays [67, 68], and the determination of the quantity  $y_{CP}$  from the  $D \rightarrow K\pi$ ,  $KK$  decays [69]. Once the  $D$  meson mixing is realized, relevant data, such as those associated with the coefficient ratio  $q/p$ , can be used to constrain new physics models [70–85]. Our formalism is expected to have

potential and broad applications in phenomenology.

### Acknowledgement

We are grateful for helpful discussions with A. Lenz, H. Umeeda, F.R. Xu and F.S. Yu. This work was supported in part by National Science and Technology Council of the Republic of China under Grant No. MOST-110-2811-M-001-540-MY3.

- 
- [1] Y. Amhis *et al.* [HFLAV], [arXiv:2206.07501 [hep-ex]].
- [2] H. Georgi, Phys. Lett. B **297**, 353 (1992).
- [3] T. Ohl, G. Ricciardi and E. H. Simmons, Nucl. Phys. B **403**, 605 (1993).
- [4] S. L. Glashow, J. Iliopoulos and L. Maiani, Phys. Rev. D **2**, 1285 (1970).
- [5] E. Golowich and A. A. Petrov, Phys. Lett. B **625**, 53 (2005).
- [6] I. I. Bigi and N. G. Uraltsev, Nucl. Phys. B **592**, 92 (2001).
- [7] A. F. Falk, Y. Grossman, Z. Ligeti and A. A. Petrov, Phys. Rev. D **65**, 054034 (2002).
- [8] M. Bobrowski, A. Lenz, J. Riedl and J. Rohrwild, [arXiv:0904.3971 [hep-ph]]; JHEP **1003**, 009 (2010).
- [9] L. Wolfenstein, Phys. Lett. B **164**, 170 (1985).
- [10] J. F. Donoghue, E. Golowich, B. R. Holstein and J. Trampetic, Phys. Rev. D **33**, 179 (1986).
- [11] P. Colangelo, G. Nardulli and N. Paver, Phys. Lett. B **242**, 71 (1990).
- [12] F. Buccella, M. Lusignoli, G. Miele, A. Pugliese and P. Santorelli, Phys. Rev. D **51**, 3478 (1995).
- [13] F. Buccella, M. Lusignoli and A. Pugliese, Phys. Lett. B **379**, 249 (1996).
- [14] T. A. Kaeding, Phys. Lett. B **357**, 151 (1995).
- [15] A. F. Falk, Y. Grossman, Z. Ligeti, Y. Nir and A. A. Petrov, Phys. Rev. D **69**, 114021 (2004).
- [16] H. Y. Cheng and C. W. Chiang, Phys. Rev. D **81**, 114020 (2010).
- [17] M. Gronau and J. L. Rosner, Phys. Rev. D **86**, 114029 (2012).
- [18] H. Y. Jiang, F. S. Yu, Q. Qin, H. n. Li and C. D. Lü, Chin. Phys. C **42**, 063101 (2018).
- [19] V. Bhardwaj, M. Dorigo and F. S. Yu, [arXiv:1901.08131 [hep-ex]].
- [20] H. Umeeda, PoS **CKM2021**, 150 (2023) [arXiv:2201.00574 [hep-ph]].
- [21] H. n. Li, H. Umeeda, F. Xu and F. S. Yu, Phys. Lett. B **810**, 135802 (2020).
- [22] H. Y. Cheng, Phys. Rev. D **26**, 143 (1982).
- [23] A. J. Buras, W. Slominski and H. Steger, Nucl. Phys. **B245**, 369 (1984).
- [24] A. Datta and D. Kumbhakar, Z. Phys. C **27**, 515 (1985).
- [25] G. Burdman, [arXiv:hep-ph/9407378 [hep-ph]].
- [26] H. n. Li and H. Umeeda, Phys. Rev. D **102**, 094003 (2020).
- [27] H. n. Li and H. Umeeda, Phys. Rev. D **102**, 114014 (2020).
- [28] H. n. Li, Phys. Rev. D **104**, 114017 (2021).
- [29] H. n. Li, Phys. Rev. D **106**, 034015 (2022).
- [30] M. Beneke, G. Buchalla and I. Dunietz, Phys. Rev. D **54**, 4419 (1996); [erratum: Phys. Rev. D **83**, 119902 (2011)].
- [31] M. Ciuchini, E. Franco, V. Lubicz, F. Mescia and C. Tarantino, JHEP **08**, 031 (2003).
- [32] A. Lenz and U. Nierste, JHEP **06**, 072 (2007).
- [33] A. J. Lenz, AIP Conf. Proc. **1026**, 36 (2008).
- [34] M. Artuso, G. Borissov and A. Lenz, Rev. Mod. Phys. **88**, 045002 (2016).
- [35] T. Jubb, M. Kirk, A. Lenz and G. Tetlalmatzi-Xolocotzi, Nucl. Phys. B **915**, 431 (2017).
- [36] R. Kingsley, S. Treiman, F. Wilczek and A. Zee, Phys. Rev. D **11**, 1919 (1975).
- [37] M. A. Shifman, A. I. Vainshtein and V. I. Zakharov, Nucl. Phys. B **147**, 385 (1979); B **147**, 448 (1979).
- [38] S. Herrlich and U. Nierste, Nucl. Phys. B **476**, 27 (1996).
- [39] A. J. Buras, D. Guadagnoli and G. Isidori, Phys. Lett. B **688**, 309 (2010).
- [40] J. Brod and M. Gorbahn, Phys. Rev. Lett. **108**, 121801 (2012).
- [41] J. S. Hagelin, Nucl. Phys. B **193**, 123 (1981).
- [42] H. Forkel, Phys. Rev. D **71**, 054008 (2005).
- [43] S. Hashimoto, K. I. Ishikawa, H. Matsufuru, T. Onogi, S. Tominaga and N. Yamada, Phys. Rev. D **60**, 094503 (1999).
- [44] N. Carrasco *et al.* [ETM], Phys. Rev. D **92**, 034516 (2015).
- [45] A. Bazavov *et al.* [Fermilab Lattice and MILC], Phys. Rev. D **93**, 113016 (2016).
- [46] R. J. Dowdall, C. T. H. Davies, R. R. Horgan, G. P. Lepage, C. J. Monahan, J. Shigemitsu and M. Wingate, Phys. Rev. D **100**, 094508 (2019).
- [47] R.L. Workman *et al.* (Particle Data Group), Prog. Theor. Exp. Phys. 2022, 083C01 (2022).
- [48] E. Golowich and A. A. Petrov, Phys. Lett. B **427**, 172 (1998).
- [49] A. Lenz, M. L. Piscopo and C. Vlahos, Phys. Rev. D **102**, 093002 (2020).

- [50] N. Carrasco, M. Ciuchini, P. Dimopoulos, R. Frezzotti, V. Gimenez, V. Lubicz, G. C. Rossi, F. Sanfilippo, L. Silvestrini, S. Simula, *et al.*, Phys. Rev. D **90**, 014502 (2014).
- [51] A. Bazavov, C. Bernard, C. M. Bouchard, C. C. Chang, C. DeTar, D. Du, A. X. El-Khadra, E. D. Freeland, E. Gámiz, S. Gottlieb, *et al.*, Phys. Rev. D **97**, 034513 (2018).
- [52] A. L. Kagan and L. Silvestrini, Phys. Rev. D **103**, 053008 (2021).
- [53] P. Ball, J. Phys. G **34**, 2199 (2007).
- [54] Z. z. Xing and S. Zhou, Phys. Rev. D **75**, 114006 (2007).
- [55] A. J. Buras, M. Jamin and P. H. Weisz, Nucl. Phys. B **347**, 491 (1990).
- [56] M. Gerlach, U. Nierste, V. Shtabovenko and M. Steinhauser, JHEP **04**, 006 (2022).
- [57] A. J. Lenz, Phys. Rev. D **84**, 031501 (2011).
- [58] C. K. Chua, W. S. Hou and C. H. Shen, Phys. Rev. D **84**, 074037 (2011).
- [59] M. Shifman, A. Vainshtein and V. Zakharov, Nucl. Phys. **B120**, 316 (1977).
- [60] J. F. Donoghue, Phys. Rev. D **30**, 1499 (1984).
- [61] M. Bobrowski, A. Lenz and T. Rauh, [arXiv:1208.6438 [hep-ph]].
- [62] M. Beneke, G. Buchalla, C. Greub, A. Lenz and U. Nierste, Nucl. Phys. B **639**, 389 (2002).
- [63] A. G. Grozin, T. Mannel and A. A. Pivovarov, Phys. Rev. D **96**, 074032 (2017).
- [64] M. Gerlach, U. Nierste, V. Shtabovenko and M. Steinhauser, Phys. Rev. Lett. **129**, 102001 (2022).
- [65] J. Brod, S. Kvedaraite, Z. Polonsky and A. Youssef, JHEP **12**, 014 (2022).
- [66] A. A. Petrov, Phys. Rev. D **56**, 1685 (1997).
- [67] M. Rama, Phys. Rev. D **89**, 014021 (2014).
- [68] S. Harnew and J. Rademacker, JHEP **03**, 169 (2015).
- [69] A. J. Schwartz, [arXiv:2207.11867 [hep-ph]].
- [70] G. Burdman, AIP Conf. Proc. **349**, 409 (1996).
- [71] R. S. Chivukula and E. H. Simmons, Phys. Rev. D **82**, 033014 (2010).
- [72] A. Faessler, T. Gutsche, S. Kovalenko, V. E. Lyubovitskij and I. Schmidt, Phys. Rev. D **82**, 075012 (2010).
- [73] J. I. Aranda, F. Ramirez-Zavaleta, J. J. Toscano and E. S. Tututi, J. Phys. G **38**, 045006 (2011).
- [74] A. J. Buras, G. Isidori and P. Paradisi, Phys. Lett. B **694**, 402 (2011).
- [75] M. Trott and M. B. Wise, JHEP **11**, 157 (2010).
- [76] Y. Adachi, N. Kurahashi, C. S. Lim and N. Maru, JHEP **01**, 047 (2012).
- [77] S. Nandi and D. London, Phys. Rev. D **85**, 114015 (2012).
- [78] J. P. Lee, [arXiv:1307.6340 [hep-ph]].
- [79] X. D. Cheng, X. Q. Li, Y. D. Yang and X. Zhang, J. Phys. G **42**, 125005 (2015).
- [80] C. Hati, G. Kumar and N. Mahajan, JHEP **01**, 117 (2016).
- [81] Q. Y. Hu, X. Q. Li, Y. D. Yang and M. D. Zheng, JHEP **06**, 133 (2019).
- [82] S. Descotes-Genon, J. Matias and J. Virto, Phys. Rev. D **85**, 034010 (2012).
- [83] A. J. Buras, P. Colangelo, F. De Fazio and F. Lopolcaro, JHEP **10**, 021 (2021).
- [84] V. Oliveira and C. A. d. S. Pires, [arXiv:2208.00420 [hep-ph]].
- [85] A. E. Cárcamo Hernández, L. Duarte, A. S. de Jesus, S. Kovalenko, F. S. Queiroz, C. Siqueira, Y. M. Oviedo-Torres and Y. Villamizar, [arXiv:2208.08462 [hep-ph]].